Available online at www.CivileJournal.org

Civil Engineering Journal

(E-ISSN: 2476-3055; ISSN: 2676-6957)

Vol. 12, No. 05, May, 2026

Artificial Neural Network and Reliability-Based Design of Concrete Beams Reinforced by FRP Bars

Hau Tran [1, 2*], Trung Nguyen-Thoi [3, 4], Quang-Thien-Buu Nguyen [5]

[1] *Laboratory for Computational Civil Engineering, Institute for Computational Science and Artificial Intelligence, Van Lang University, Ho Chi Minh City 70000, Vietnam.*

[2] *Faculty of Civil Engineering, Van Lang School of Technology, Van Lang University, Ho Chi Minh City 70000, Vietnam.*

[3] *Laboratory for Applied and Industrial Mathematics, Institute for Computational Science and Artificial Intelligence, Van Lang University, Ho Chi Minh City 70000, Vietnam.*

[4] *Faculty of Mechanical, Electrical, and Computer Engineering, Van Lang School of Technology, Van Lang University, Ho Chi Minh City 70000, Vietnam.*

[5] *Department of Civil and Environmental Engineering, Seoul National University, Seoul, South Korea.*

Received 02 February 2026; Revised 23 April 2026; Accepted 28 April 2026; Published 01 May 2026

Abstract

FRP bars have been utilized widely to replace steel bars in concrete beams due to their excellent corrosion resistance. Therefore, this paper aims to propose an efficient procedure based on artificial neural network (ANN) and reliability analysis to predict the moment capacity, the failure modes, and the resistance reduction factor for the design of concrete beams reinforced by FRP bars. In particular, 200 FRP RC beams are collected to train and verify the ANN model. In addition, a source code based on the Monte Carlo method is developed in MATLAB for the reliability analysis. The ANN model and the Matlab code are integrated to determine the failure probability, the reliability index, and the resistance reduction factor of FRP RC beams by rigorously considering the uncertainty of numerous variables. According to the findings of this study, ANN can be applied to predict the ultimate moment of FRP RC beams well since the mean and *CoV* of the model error are only 0.98 and 0.12, respectively, which are better than those obtained from ACI 440.1R. Furthermore, the resistance reduction factors for the design of FRP RC beams by ANN can be taken as 0.65 corresponding to the target reliability index of 4.0.

Keywords: Artificial Neural Network (ANN); Design Guideline; FRP RC Beams; Reliability Analysis; Resistance Reduction Factor.

1. Introduction

Reinforced concrete (RC) structures have been applied broadly in the civil engineering industry, and they have been investigated in numerous studies from the member level, such as columns [1-3], beams [4-6], and slabs [7], to the system level, such as frames and buildings [8, 9]. However, steel bars can be easily corroded when working in aggressive environments, which reduces structural durability and increases maintenance costs [10]. Therefore, fiber reinforced polymer (FRP) bars have been widely used as an alternative to steel reinforcement in concrete structures due to their various advantages such as light weight, high strength, and excellent corrosion resistance.

* Corresponding author: hau.tranquang@vlu.edu.vn

https://doi.org/10.28991/CEJ-2026-012-05-05

To better understand the behavior and develop design standards for FRP RC structures, many studies have been conducted, including both experiments [11-13] and numerical simulations [14-16]. Among these, FRP RC beams have attracted significant attention from researchers. Although experimental testing provides the most reliable observations about practical behaviors of FRP RC beams, it is time consuming and expensive. Another approach is to employ numerical simulation such as finite element analysis to analyze the response of FRP RC beams under loading conditions. This approach can effectively capture crucial features, including ultimate load, deformation, failure modes, and crack patterns. However, issues such as long computational time, convergence difficulties, and software license cost can be big challenges. Recently, artificial neural networks (ANNs) have emerged as a promising approach and have been applied to explore the response of FRP RC beams [17-20]. This method can surpass the drawbacks mentioned above. ANN models mimic the human brain to build computational neural networks that are able to learn and provide predictions using input data. ANN includes three types of learning processes that are supervised learning, unsupervised learning, and reinforcement learning. In supervised learning, the predicted outputs are compared directly with the actual outputs to determine the error. Unsupervised learning does not require the actual outputs, as the outputs are forecasted using the correlation of the input data. In reinforcement learning, problems involve what to do; how to map situations to actions to maximize a numerical reward signal. Generally, supervised learning is the most commonly applied to solve civil engineering problems [16, 18, 19].

Regarding reliability analysis, it is applied in many studies to determine the failure probability and reliability indices of FRP RC beams due to uncertainties of variables such as material properties, section dimensions, applied loads, and error of the prediction models. These uncertainties are represented by probabilistic models leading to a probabilistic distribution of the structural resistance. Consequently, it can result in the failure of the beams. Currently, some studies related to reliability analysis of FRP RC beams have been conducted [21-23]. Most of these studies calibrate the reliability indices of FRP beams by using the design equations given in standards, or applying numerical analysis based on commercial software. Using design equations to calculate the load-carrying capacity can reduce the computational time significantly. However, results are quite conservative, as there are many empirical coefficients and simplifying assumptions in the equations. In contrast, numerical simulation can reflect well the practical behavior of FRP RC beams and yield quite accurate load-carrying capacity. Therefore, the predicted reliability indices are also more precise. However, this method requires substantial computational resources.

Studies on the behavior and reliability analysis of FRP RC beams have been conducted by [20, 24, 25]. Murad et al. [20] employed artificial intelligence/machine learning (AI/ML) to predict the flexural capacity of concrete beams reinforced with FRP bars. In their study, an AI/ML model was built by using a database of 116 FRP RC beams. The predicted results were compared with those obtained from ACI 440 and CSA S806. Their results agreed well with those obtained from experiments, ACI 440, and CSA S806. However, the study was limited to the estimation of FRP beams' ultimate load; the reliability analysis for evaluating current design standards was not conducted. Ge et al. [24] applied an AI/ML model to predict the bending capacity of concrete beams reinforced with hybrid FRP and steel bars. Based on the results compared with experiments, their developed AI/ML model demonstrated good performance, as the predicted results agreed well with those from experiments. However, their study did not assess current design standards of FRP RC beams. Zhang et al. [26] conducted a numerical study based on AI/ML to predict the flexural capacity of concrete beams reinforced with hybrid steel and FRP bars. The outputs from the numerical model were better than those predicted by ACI 440.1.

However, reliability analysis was not carried out in their study to evaluate current design standards of FRP RC beams. In several research studies, reliability analysis of concrete beams reinforced by FRP bars was conducted to examine the safety of equations given in design standards. Particularly, Feng et al. [22] carried out reliability analysis to evaluate the design of FRP-reinforced concrete beams with compression-yielding blocks. In their study, calculation equations were established by assumptions such as strain was linearly distributed along the section and concrete tensile strength was ignored. Therefore, the prediction equations could not capture the practical behavior of FRP RC beams. The current design guidelines and standards were also not evaluated. He & Qiu [27] employed reliability analysis to assess resistance reduction factors of FRP RC beams designed by ACI 440.1. Their study utilized equations provided by the standard to conduct reliability analysis. This approach saved computational time significantly, but these equations were established using many assumptions. Consequently, the results were conservative. Other studies by Zhang et al. [26] and Zhou et al. [28] also focused on the reliability analysis of FRP concrete beams, but they targeted shear behavior. Based on the review above, it has been found that there is a lack of studies that employ ANNs to conduct reliability analysis and predict the load-carrying capacity of FRP RC beams. This method can substantially reduce the computational time while still retaining high accuracy.

Therefore, this study aims to develop a feasible and efficient procedure based on ANN and reliability analysis to predict the ultimate moment and failure mode and propose the resistance reduction factor for the design of FRP RC beams. At first, the ANN model is trained in Matlab using FRP RC beams collected from previous experimental studies. This ANN model is validated with the results from experiments and ACI 440.1R. Then a source code for the reliability analysis is developed using the Monte Carlo method. This source code is integrated with an ANN model in MATLAB to estimate ultimate moment, failure probability, and reliability index. In addition, design equations and resistance reduction factors of ACI 440.1R are also evaluated by the proposed process.

2. ANN Model for Predicting Moment Capacity of FRP RC Beams

The ANN model is developed by using available data from FRP RC beams to predict the outputs such as load-carrying capacity and failure modes. Based on this unique characteristic, ANN can overcome limitations of conventional numerical approaches, including long computational time and expensive software licensing costs. The structure of an ANN includes three main components that are the input layer, hidden layers, and output layer, as depicted in Figure 1. At the beginning of the training stage of the ANN model, the available data (x_i) will be provided to the neurons of the input layer. Then weights (w_{ij}) and bias (b_i) are applied to transfer the information to hidden layers as given in Equation 1. The output of each neuron in a hidden layer serves as input data to determine the values of neurons in the subsequent layer. Furthermore, activation functions are employed to transfer the signals among layers and yield results in the output layer. Some popular activation functions used to train the ANN models are the logistic sigmoid function (Equation 2), the hyperbolic tangent function (Equation 3), and the linear function (Equation 4) (see Figure 2).

$$S_j = \sum_{i=1}^{n} w_{ij} x_i + b_i \quad (1)$$

$$f(z) = \frac{1}{1+e^{-z}} \quad (2)$$

$$f(z) = \frac{2}{1+e^{-2z}} - 1 \quad (3)$$

$$f(z) = z \quad (4)$$

where, S_j is the value of each neuron in the hidden layer; x_i are the input values; w_{ij} and b_i are weights and bias, respectively; $f(z)$ is activation function (AF) used to transfer values in the hidden layers and output layer.

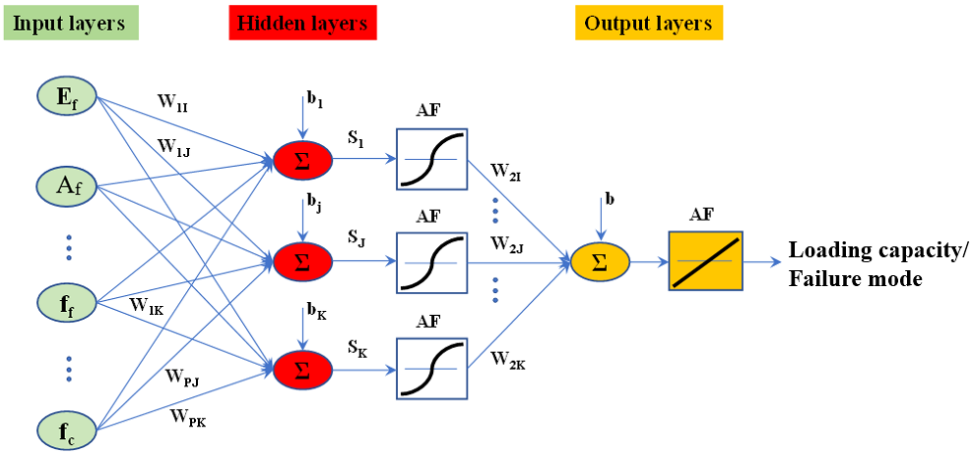

Figure 1. Typical layers of an ANN model

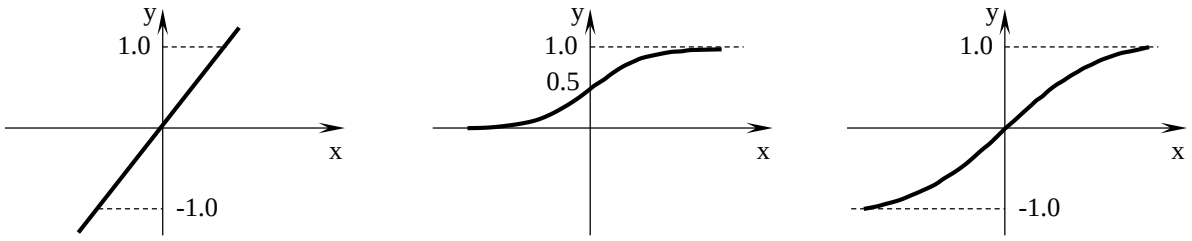

(a) Linear function (b) Logsig function (c) Tansig Function

Figure 2. Some typical activation functions

In this study, the ANN algorithm provided by MATLAB is applied to train the model for the prediction of the ultimate moments and failure modes of FRP RC beams. There are three available algorithms given in MATLAB named Levenberg-Marquardt (LM), Bayesian regularization (BR), and scaled conjugate gradient (SCG). Among the three algorithms, the LM method shows better performance in terms of convergence rate, generalization ability, and prediction accuracy compared to the other algorithms. These advantages have been demonstrated in previous studies [19, 29, 30]. Therefore, this method is adopted in this research. To train the ANN model, 200 FRP RC beams are collected from experimental studies. The parameters used for the input layer are section width b_c (mm), section height h_c (mm), concrete compressive strength f_c (MPa), area of FRP bars A_f (mm²), elastic modulus of FRP bar E_f (MPa), FRP tensile strength f_{fu} (MPa), and reinforcement-to-balanced reinforcement ratio p_f / p_{fb}. The actual outputs include ultimate moments and failure modes of FRP RC beams. It should be noted that the ANN model built in this study is applied for FRP RC beams subjected to static gravity loads. To account for other loading types such as impact loads, blast loads, or environmental

conditions, experimental data obtained from these conditions should be collected to train the ANN model. However, they are out of the scope of this study. The precision of the trained ANN model can be represented by the coefficient of determination *R*-squared (R^2), and the absolute percentage error (MAPE), which are calculated by the following equations [31]:

$$R^2 = 1 - \frac{\sum_{i=1}^{k}(Y_i - \hat{Y}_i)^2}{\sum_{i=1}^{k}(Y_i - \bar{Y})^2} \quad (5)$$

$$MAPE = \frac{1}{k}\sum_{i=1}^{k}\left|\frac{\hat{Y}_i}{Y_i} - 1\right| \quad (6)$$

where, Y_i is the measured values; $\hat{Y}_i$ is the predicted values; $\bar{Y}$ is the mean of measured values; k is the number of specimens.

3. Design by ACI 440.1R

Several standards and guidelines have been established for the design of FRP RC beams, among which ACI 440.1R [32] is one of the most widely applied design documents. In these design guidelines, the cross section of the beam is assumed to remain plane under loading conditions, and strain distributes linearly along the height of the section. In addition, to simplify the design equations, the nonlinear stress distribution of concrete along the height of the compression zone is converted to the equivalent rectangular stress block using specified coefficients (Figure 3). The ultimate moment of the FRP RC beams is strongly dependent on the types of failure modes, as the stress and strain of concrete and FRP in each failure mode are significantly different. To determine the type of failure of the beam, the reinforcement ratio (p_f) is compared with the balanced reinforcement ratio (p_{fb}) calculated by Equation 7. If $p_f/p_{fb}>1$, the failure mode is assumed to be concrete crushing. The moment capacity of this case is determined by Equation 8. If $p_f/p_{fb}<1$, the failure mode is FRP rupture. The ultimate moment is calculated by Equation 10. The values of moments in Equations 8 and 10 are multiplied with a reduction factor calculated by Equation 12 to determine the design moment capacity:

$$\rho_{fb} = \alpha_1\beta_1\frac{f_c}{f_{fu}}\frac{E_f\varepsilon_{cu}}{E_f\varepsilon_{cu}+f_{fu}} \quad (7)$$

$$M_n = A_f E_f \varepsilon_{cu}\frac{\beta_1 d - a}{a}\left(d - \frac{a}{2}\right) \quad (8)$$

$$a = \frac{A_f f_f}{0.85 f_c b} \quad (9)$$

$$M_n = A_f f_{fu}\left(d - \frac{\beta_1 c_b}{2}\right) \quad (10)$$

$$c_b = \left(\frac{\varepsilon_{cu}}{\varepsilon_{cu}+\varepsilon_{fu}}\right)d \quad (11)$$

$$\phi = \begin{cases} 0.55 & for\ \rho_f \le \rho_{fb} \\ 0.3 + 0.25\frac{\rho_f}{\rho_{fb}} & for \rho_{fb} < \rho_f < 1.4\rho_{fb} \\ 0.65 & for\ \rho_f \ge 1.4\rho_{fb} \end{cases} \quad (12)$$

where, f_c is the compressive strength of concrete (MPa); f_{fu} is the tensile strength of FRP bars (MPa); E_f is the elastic modulus of FRP bars (MPa); ε_{cu} is the ultimate compressive strain of concrete; ε_{fu} is the ultimate tensile strain of FRP bars; A_f is the area of FRP bars (mm^2); b is the width of the beam section (mm); d is the effective depth of the beam section (mm); α_1 and β_1 are coefficients to transform the actual concrete compressive stress distribution to an equivalent rectangular stress block.

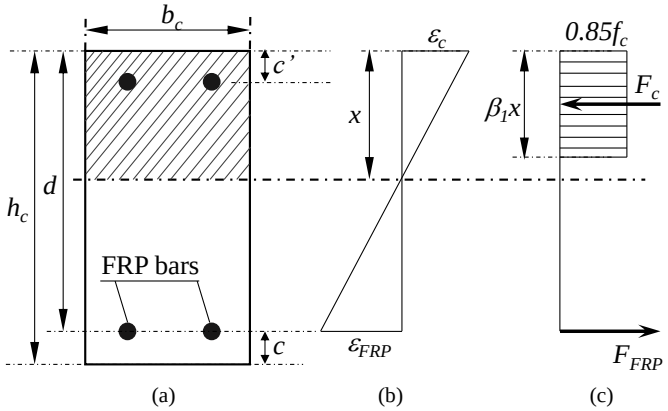

Figure 3. Stress and strain distribution along the section of FRP RC beams: a) cross section; b) strain distribution; c) stress distribution

4. Test Database and Model Error

Many experimental studies have been conducted to investigate the flexural behavior of FRP RC beams, focusing on load-carrying capacity, crack formation, deformation, and failure modes [33–40]. The flexural behavior of FRP RC beams can be evaluated using either three-point or four-point bending tests. However, four-point bending tests are generally preferred because they provide a clearer representation of failure modes and crack propagation, as reported in several studies [37, 41]. Based on these experimental investigations, a database of 200 FRP RC beams was compiled, including two typical failure modes: concrete crushing and FRP rupture. Approximately 76% of the collected specimens (around 154 beams) exhibited concrete crushing failure. In contrast, FRP rupture is generally avoided because it leads to a more brittle failure mode. Consequently, this type of failure is not recommended in some design standards, such as CSA S806.

The distributions of concrete compressive strength f_c, FRP tensile strength f_{fu}, section width b_c, section height h_c, and FRP elastic modulus E_f for the collected beams are presented in Figure 4. As shown in Figure 4a, the section widths range from 100 mm to 500 mm, with approximately 93% of the specimens falling between 100 mm and 250 mm. The section heights vary from 150 mm to 550 mm, with nearly 75% of the beams having heights between 200 mm and 400 mm (Figure 4b). Figure 4c shows that the concrete compressive strength ranges from 20 MPa to 102 MPa, while about 90% of the values lie between 25 MPa and 55 MPa. The tensile strength of FRP bars ranges from 520 MPa to 2069 MPa, with around 70.5% of the values between 520 MPa and 1200 MPa (Figure 4d). Similarly, the elastic modulus of FRP bars varies widely from 36 GPa to 200 GPa, although nearly 75% of the values fall between 36 GPa and 60 GPa (Figure 4e). Figure 4f illustrates that the ratio p_f/p_{fb} ranges from 0.6 to 10, while most tested beams have values lower than 5. Therefore, the collected dataset of FRP RC beams covers a wide range of parameters and can serve as a reliable source for training the ANN model.

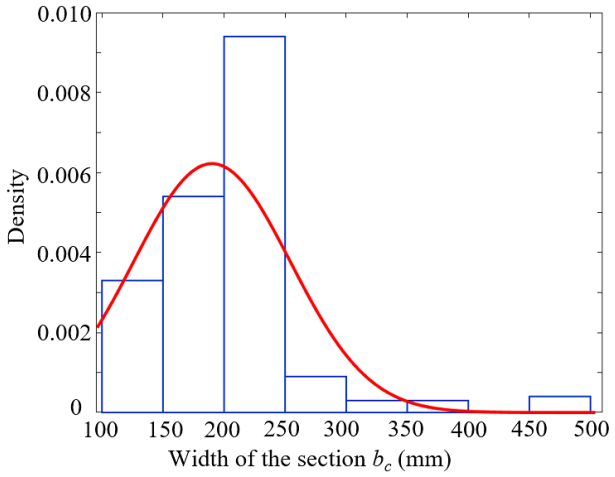

a) Width of the section

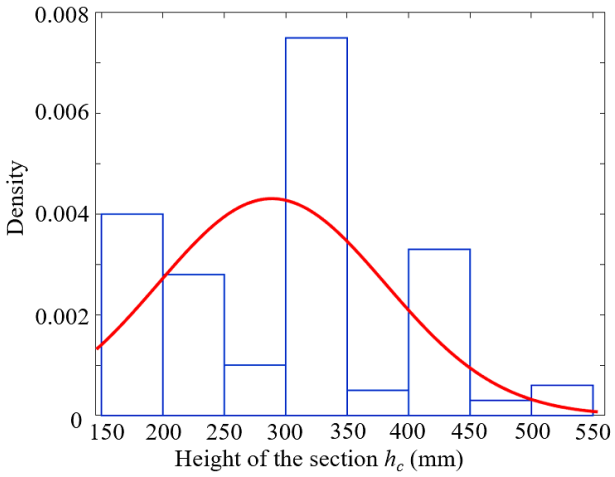

b) Height of the section

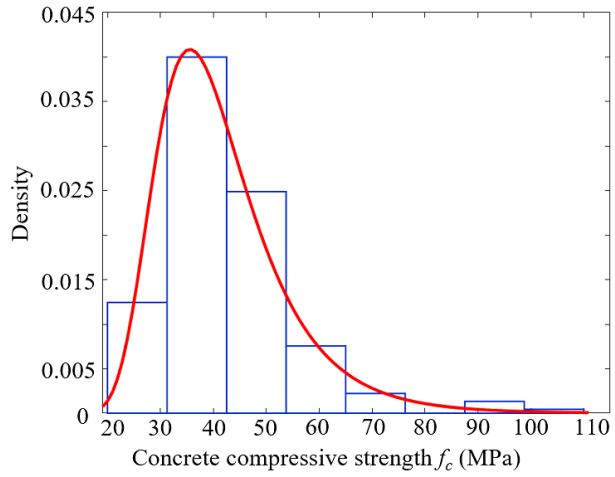

c) Concrete compressive strength

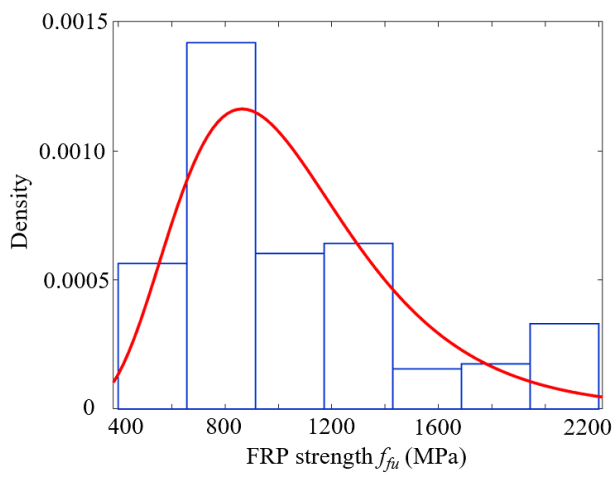

d) FRP tensile strength

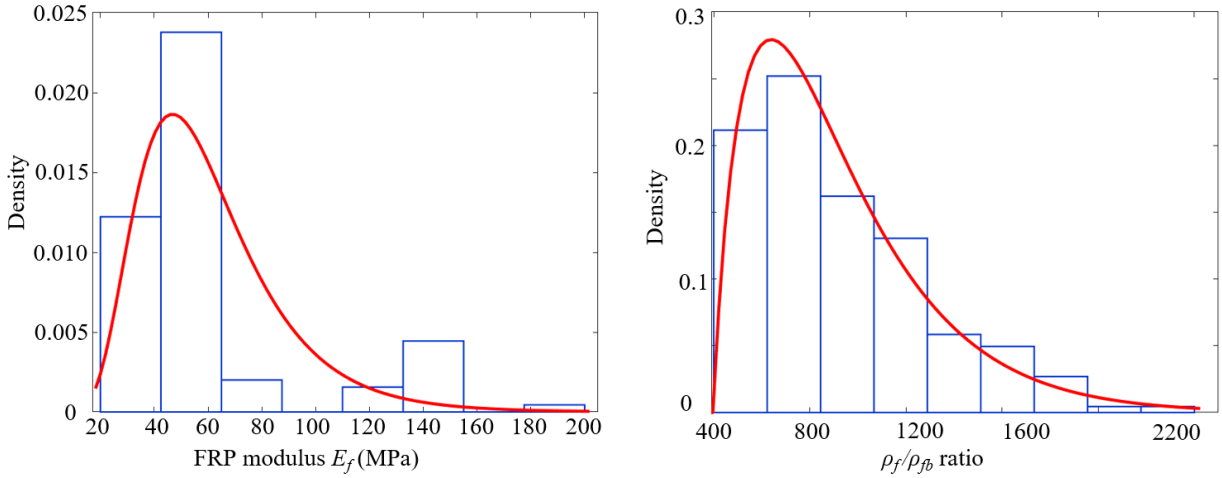

e) FRP elastic modulus **f) Reinforcement-to-Balance reinforcement ratio**

Figure 4. Distribution of some main parameters of the tested FRP RC beams

Out of the 200 collected beams, 150 specimens were used to train the ANN model, while the remaining 50 beams were used to validate the model and evaluate its prediction error. The results of the trained ANN model are presented in Table 1 and Figure 5. As shown in Figure 5-a, the trained ANN model predicts the ultimate moment capacity of FRP RC beams with high accuracy, achieving an R^2 value of 0.966 and a MAPE of 0.11. These values indicate strong predictive performance of the ANN model.

It should be noted that no official threshold values for R^2 and MAPE are specified in current design standards. ANN models are generally trained to avoid overfitting and to achieve high R^2 values and low MAPE values, since higher R^2 and lower MAPE indicate greater prediction accuracy. In general, acceptable ranges for R^2 and MAPE are approximately 0.90–0.99 and 1%–10%, respectively, as reported in various studies [17, 24, 29].

Table 1 and Figure 5-b compare the failure modes predicted by the ANN model with those observed experimentally. For concrete crushing, the trained ANN model correctly predicted 100% of the cases, corresponding to 109 beams. In the case of FRP rupture, 92.7% of the failure modes predicted by the ANN model matched the experimental results (Figure 5-b). The relatively lower prediction accuracy for FRP rupture compared to concrete crushing can be attributed to the smaller number of FRP rupture specimens in the dataset. In addition, the limited amount of data within the transition zone ($1.0 < p_f/p_{fb} < 1.4$), where FRP rupture is more likely to occur, also contributes significantly to this difference in prediction accuracy.

To evaluate the prediction error of both the ANN model and ACI 440.1R, each method was applied to estimate the ultimate moment of 50 beams whose section dimensions, material properties, and ultimate moments are listed in Table 2. For the ANN model, the mean and coefficient of variation (CoV) of the model error were 0.98 and 0.12, respectively. Based on distribution fitting in MATLAB, the Gumbel distribution was found to provide the best fit for the ANN model error, as shown in Figure 6-a. For ACI 440.1R, the Gumbel distribution also provided the best fit, with a mean and CoV of 0.97 and 0.17, respectively (Figure 6-b).

The values of the mean and CoV clearly indicate that the ANN model predicts the moment capacity of FRP RC beams more accurately than the design equations of ACI 440.1R. Since the ANN model reduces the CoV of the test-to-prediction moment ratio compared to ACI 440.1R, it can improve the reliability index of the investigated beams. Therefore, the ANN model developed in this study has the potential to enhance practical design compared to ACI 440.1R. Additional details are provided in Figure 7, where the values of M_{test}/M_{ANN} are distributed within a narrower range than those of M_{test}/M_{ACI}. Specifically, almost all M_{test}/M_{ANN} ratios fall within the range of 0.8 to 1.2, whereas M_{test}/M_{ACI} values fluctuate over a wider range of 0.75 to 1.35.

Table 1. Failure modes of FRP RC beams obtained from experiments and ANN

Failure mode	Number of beams from test	Number of beams predicted by ANN	Percentage (%)
Concrete crushing	109	109	100
FRP rupture	41	38	92.7

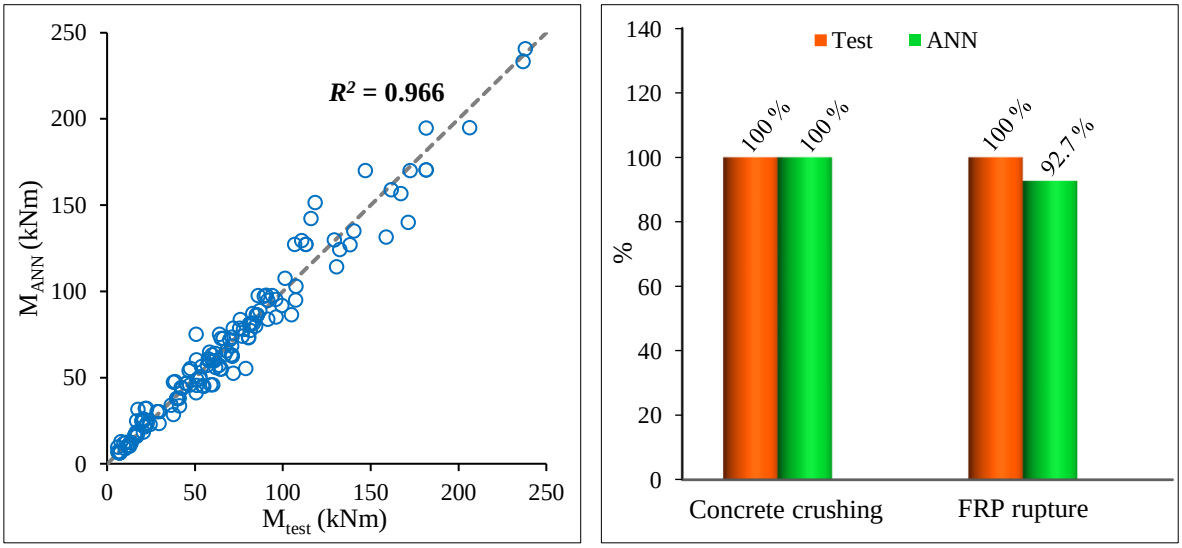

a) Moment capacity **b) Failure mode**

Figure 5. Moment capacity and failure modes of the trained data predicted by ANN

Table 2. Ultimate moments predicted by ANN and ACI 440.1R

Specimen	b_c (mm)	h_c (mm)	f_c (MPa)	A_f (mm^2)	E_f (GPa)	f_{fu} (MPa)	M_{test} (kNm)	M_{test} /M_{ANN}	M_{test} /M_{ACI}	Ref.
2T10B	180	230	30	157.1	50.0	1190	23.44	1.20	0.98	
2T12B	180	230	30	226.2	50.0	1190	31.13	1.23	1.12	Abed et al. [33]
3T16B	180	230	30	603.2	50.0	1190	38.06	1.01	0.94	
SA-B10-1	125	200	33.12	157.1	56.0	1565	14.95	1.15	0.91	
SA-B10-2	125	200	33.12	157.1	56.0	1565	15.43	1.19	0.94	Shamass & Cashell [38]
R-B10-1	125	200	35.52	157.1	54.0	1356	15.54	0.83	0.93	
R-B10-2	125	200	35.52	157.1	54.0	1356	15.50	0.83	0.93	
N-2#12-10-3.05	150	200	41.01	226.2	49.3	1075	24.47	0.97	1.11	
N-4#12-10-3.13	150	200	41.01	452.4	49.3	1075	27.77	1.07	0.96	
N-2#12-8-2.69	150	220	41.01	226.2	49.3	1075	25.36	0.84	0.97	
N-4#12-10-2.78	150	220	41.01	452.4	49.3	1075	32.56	0.98	0.94	Wang et al. [40]
N-2#14-8-2.70	150	220	41.01	307.9	51.7	1102	32.96	0.94	1.09	
N-4#14-10-2.78	150	220	41.01	615.8	51.7	1102	36.25	1.35	0.92	
N-5#12-10-2.51	150	250	41.01	565.5	49.3	1075	37.90	0.90	0.80	
NB#10	200	300	34.4	166.3	43.9	1003.4	37.60	0.84	0.91	
NB#12	200	300	34.4	267.5	45.7	983.5	53.20	1.00	1.03	
NB3#10	200	300	34.4	249.5	43.9	1003.4	50.80	0.98	1.03	
NB#16	200	300	34.4	452.9	49.2	988.5	61.10	0.90	0.92	Mostafa et al. [37]
NGI#12	200	300	34.4	274.1	48.5	951.4	50.30	0.94	0.94	
NGII#12	200	300	34.4	294.8	48.3	980.2	52.10	0.93	0.95	
NGIII#12	200	300	34.4	300.4	49.0	980.7	51.60	0.92	0.92	
COMP-00	200	240	35.3	508.1	43.4	885	41.37	1.02	0.92	
COMP-25	200	240	35.3	508.1	43.4	885	39.06	0.96	0.87	Almusallam et al. [39]
COMP-50	200	240	36.4	508.1	43.4	885	39.35	0.96	0.86	
COMP-75	200	240	36.4	508.1	43.4	885	40.60	0.99	0.89	
ISO2	200	300	43	573.0	45.0	600	80.40	1.11	1.04	
ISO3	200	550	43	573.0	45.0	600	181.70	1.08	1.08	Benmokrane et al. [34]
ISO4	200	550	43	573.0	45.0	600	181.70	1.08	1.08	

N2#13G2	200	400	33.5	261.2	67.0	1639	82.78	0.94	0.85	El-Nemr et al. [36]
N3#13G1	200	400	33.5	384.9	48.7	817	81.34	1.06	0.82	
H2#13G2	200	400	59.1	261.2	67.0	1639	101.59	1.04	0.85	
H3#13G1	200	400	59.1	384.9	48.7	817	85.58	0.94	0.76	
N5#15G2	200	400	29	970.4	69.3	1362	129.32	1.00	0.84	
N6#15G1	200	400	33.5	1161.9	50.0	762	118.73	0.79	0.76	
H5#15G2	200	400	73.4	970.4	69.3	1362	178.00	1.04	0.74	
H6#15G1	200	400	73.4	1161.9	50.0	762	177.73	0.91	0.79	
N5#15G3	200	400	33.8	970.4	59.5	1245	110.58	0.86	0.70	
N2#25G3	200	400	33.8	1019.3	60.3	906	115.93	0.82	0.72	
H5#15G3	200	400	73.4	1040.0	59.5	1245	188.37	1.07	0.81	
H2#25G3	200	400	73.4	1019.3	60.3	906	189.06	1.08	0.82	
N-212-D1-A	140	190	32.1	226.2	63.4	1321	24.51	1.00	1.28	Barris et al. [35]
N-212-D1-B	140	190	32.1	226.2	63.4	1321	23.85	0.98	1.25	
N-216-D1-A	140	190	32.1	402.1	64.6	1015	29.82	0.80	1.26	
N-216-D1-B	140	190	32.1	402.1	64.6	1015	29.79	0.79	1.26	
N-316-D1-A	140	190	32.1	603.2	64.6	1015	31.49	0.95	1.16	
N-316-D1-B	140	190	32.1	603.2	64.6	1015	33.13	0.99	1.22	
N-212-D2-A	160	190	32.1	226.2	63.4	1321	21.96	0.87	1.06	
N-212-D2-B	160	190	32.1	226.2	63.4	1321	21.96	0.87	1.06	
H-316-D1-A	140	190	54.5	603.2	64.6	1015	45.00	1.07	1.30	
H-316-D1-B	140	190	54.5	603.2	64.6	1015	44.44	1.05	1.29	
							Mean	0.98	0.97	
							CoV	0.12	0.17	

Notes: b_c is width of beams; h_c is height of beams; f_c is concrete compressive strength; A_f is total area of tensile reinforcement; E_f is modulus of reinforcement; f_{fu} is tensile strength of reinforcement; M_{test} is experimental ultimate moment; M_{ANN} is ultimate moment from ANN; M_{ACI} is ultimate moment from ACI.

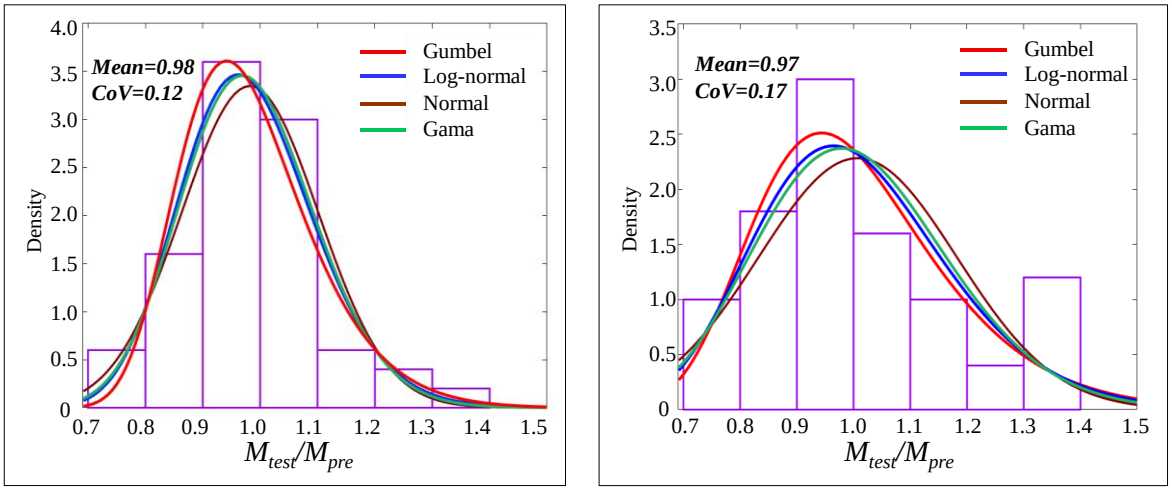

a) ANN **b) ACI 440.1R**

Figure 6. Model error of ultimate moments predicted by ANN model and ACI 440.1R

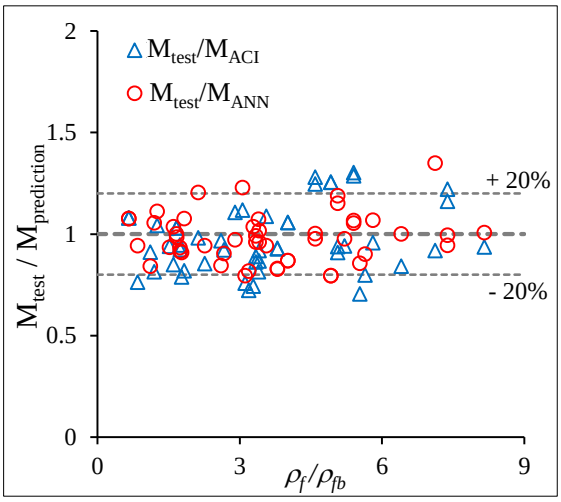

Figure 7. Comparison between M_{test} and $M_{prediction}$

5. Reliability Analysis

In the design of FRP RC beams, the nominal values of material properties, geometries, and applied loads are used to compute the ultimate moment. However, uncertainties arising from material production, casting specimens, or measurement introduce variability into these nominal values. It causes the fluctuation in the value of not only applied loads but also the ultimate moments, as shown in Figure 8. In this figure, examples on the distributions of applied moment and the moment capacity of the beam are illustrated. Due to uncertainties mentioned above, applied moment and ultimate moment distribute in a certain range with a particular type of probabilistic model. Consequently, the designed beams fail when the applied moment and the moment capacity intersect with each other, as can be seen from Figure 8. This region is named as the failure region (Figure 8-b), and the target of the reliability analysis is to determine the probability of this failure region, which is named as the failure probability. The details about the probabilistic models of random variables are presented in Tran & Nguyen-Thoi [5].

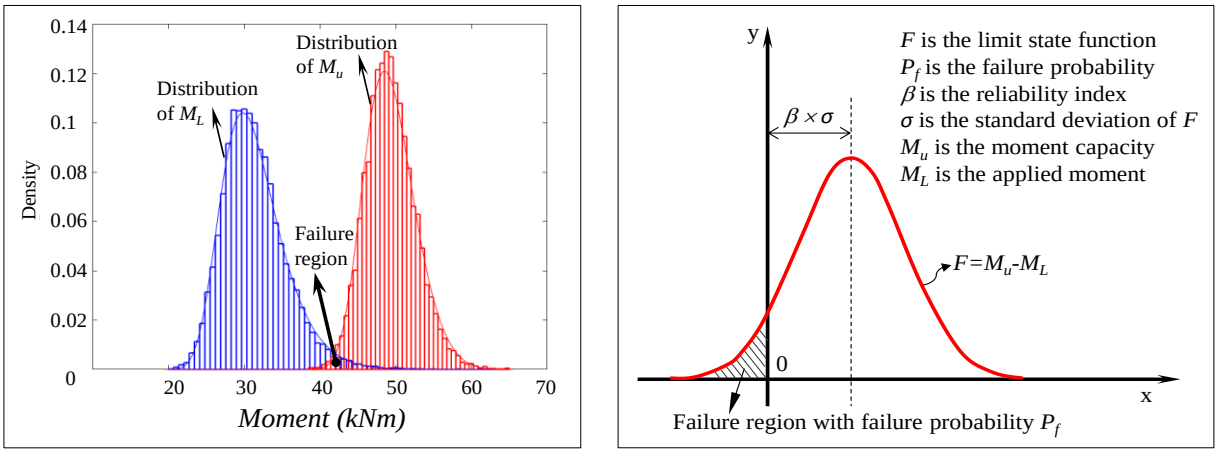

(a) Distribution of M_u and M_L **(b) Failure region of the limit state function F**

Figure 8. Failure region caused by the uncertainty of random variables

In this section, an efficient reliability analysis procedure based on the trained ANN model and the design equations of ACI 440.1R is established. The reliability analysis is to determine the probability of this failure region, as illustrated in Equation 13.

$$P_f = P_r[F(z_1,\ z_2,\ldots,\ z_n) \le 0] \tag{13}$$

where, P_f is the failure probability; P_r is the probability of the event in the bracket; F is the limit state function; z_1, z_2, …, z_n are random variables. In the case of FRP RC beams, the limit state function is established using the applied moment and the ultimate moment as shown in Equation 14.

$$F = ME \times M_u - M_L \tag{14}$$

where, ME is the model error; M_u is the ultimate moment of FRP RC beams (kNm); M_L is the moment caused by the applied loads (kNm). To solve Equation 13, Monte – Carlo method is applied in this study as this approach is feasible and efficient to apply to any kind of structures. Based on this method, the failure probability, the reliability index and the resistance reduction factor of the investigated FRP RC beams designed by ANN and ACI 440.1R are illustrated in Figure 9. The details of this figure can be explained as follows:

(i) For each FRP RC beam, the moment caused by the applied loads M_L is calculated. Then ANN and ACI 440.1R are employed to compute the value of ultimate moment named as M_{u_ANN} and M_{u_ACI}, respectively. The load factors are determined by Equation 15.

$$\lambda_{ANN} = \frac{M_{u\_ANN}}{M_L},\ \lambda_{ACI} = \frac{M_{u\_ACI}}{M_L} \tag{15}$$

After that, N samples of the investigated beams are generated using the probabilistic models of variables given in Tran and Nguyen-Thoi [5]. Based on the trained ANN model and ACI 440.1R, the ultimate moment of each sample is calculated. Then these values are substituted into Equation 14 to find the value of the limit state function F.

(ii) If $F \le 0$, the sample fails. All the failed samples (N_f) are counted. After that, the failure probability and reliability index are determined by Equations 16 and 17, respectively. The values of load factors in step (i) and the reliability index are recorded.

$$P_f = \frac{N_f}{N} \quad (16)$$

$$\beta = -\Phi^{-1}(P_f) \quad (17)$$

(iii) Applied loads are scaled and turn back to step (i) to get new values of load factors.

(iv) Steps (i) to (iii) are iterated until β–λ curve intersects with $\beta=\beta_T$. Determine the load factor corresponding to β_T, the value of resistance reduction factor for the design is computed by Equation 18.

$$\phi_{design} = \frac{1}{\lambda_T} \quad (18)$$

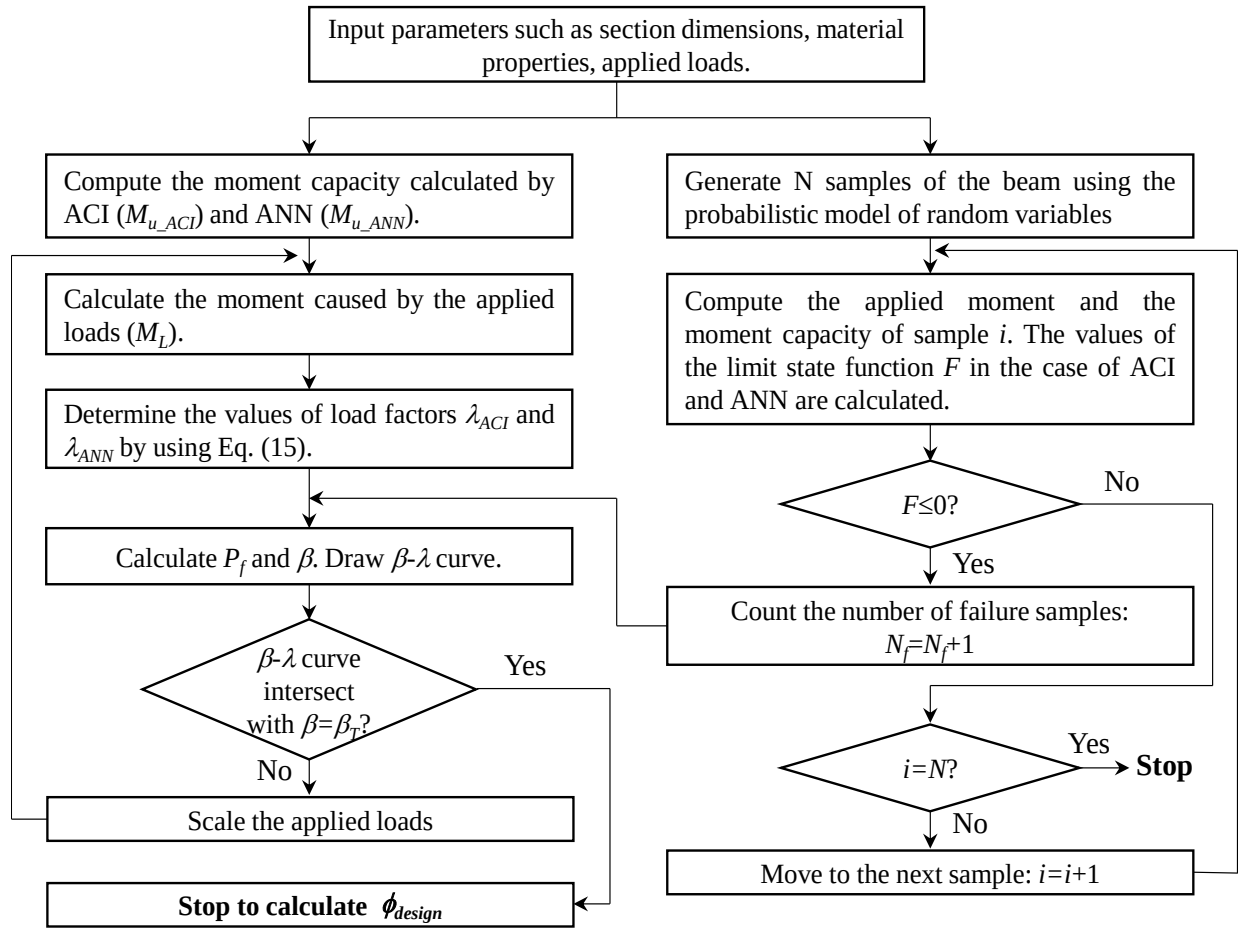

Figure 9. Reliability analysis based on Monte Carlo method and ANN

In MC method, the accuracy of the predicted failure probability and reliability index is dependent on the number of generated samples (N) as indicated in Equation 19. To explore the effects of N on the reliability index and the analysis time, two beams named as COMP–00 and 2T10B are analyzed. Results of the analysis are depicted in Figure 10. It is obvious that reliability indices are highly sensitive to N at lower sample sizes as can be seen from Figure 10-a. Particularly, when N=10^3 samples, the reliability indices of specimens COMP-00_ANN, COMP-00_ACI, 2T10B_ANN, and 2T10B_ACI are approximately 2.93, 3.38, 3.52, and 3.51, respectively. However, when the value of N is 10^6 samples, the reliability indices of these samples are about 3.0, 3.18, 3.57, and 4.06, respectively, indicating a maximum fluctuation of up to 15.67 % (from 3.51 to 4.06). In contrast, when the value of N rises from 10^6 to 2.5×10^6 samples, the values of reliability indices of specimens COMP-00_ANN, COMP-00_ACI, 2T10B_ANN, and 2T10B_ACI stabilize with minor variations from 3.0 to 3.02, 3.18 to 3.22, 3.57 to 3.58, and 4.06 to 4.08, respectively. Therefore, the number of samples plays an important role, and it must be selected to ensure the *Error* in Equation 19 remains below 10 %. The influence of N on the calculation time is demonstrated in Figure 10-b. It is obvious that when the value of N increases from 5×10^5 to 2.5×10^6 samples, the computational time rises significantly from approximately 135 (*s*) to 900 (*s*). Therefore, choosing an appropriate value of N is important to balance the accuracy and the computational efficiency. This figure also demonstrates that the analysis time in the case of ACI is comparable to that in the case of ANN, which implies that the application of ANN can save the calculation time of the reliability analysis significantly compared to finite element method or discrete element method.

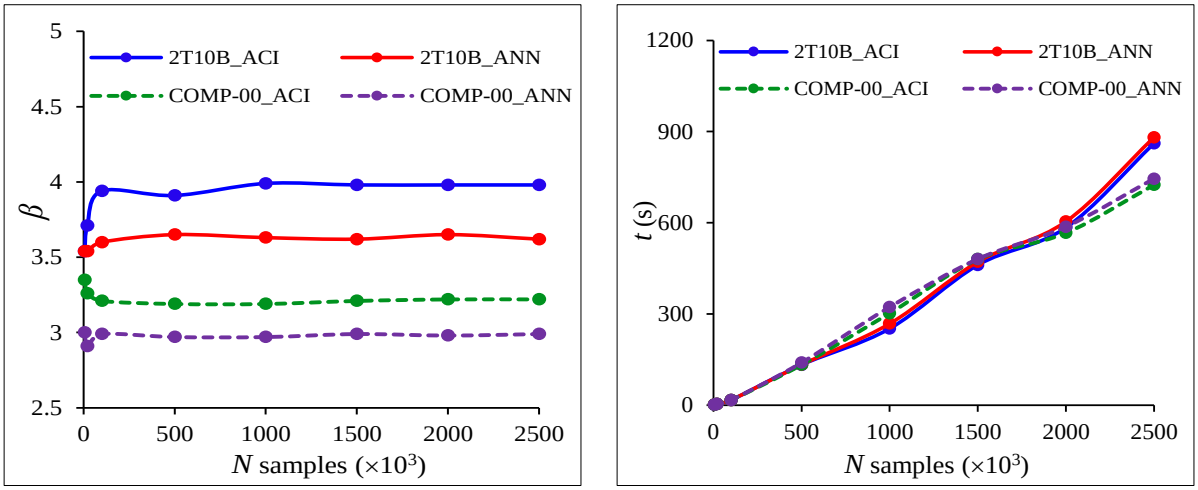

(a) Effects of number of samples on reliability indices

(b) Effects of number of samples on calculation time

Figure 10. The effect of number of samples on reliability indices and calculation time

6. Results and Discussion

Table 3 demonstrates an example of the load-scaling process to determine the β–λ curves of beam COMP–00 based on the proposed ANN-MC reliability analysis procedure. The section dimension of this beam is 200×240 mm with concrete compressive strength of 35.3 MPa. The tensile strength, elastic modulus, and area of FRP bars are 885 MPa, 43.3 GPa, and 508.1 mm^2, respectively. The moment caused by external loads at the mid-span of the beam is 24.76 kNm. This value of the applied moment is then scaled up by factors of 1.27, 1.45, and 1.64 to achieve new applied moments of 31.52 kNm, 36.02 kNm, and 40.52 kNm, respectively, as can be seen from Table 3. Corresponding to applied moments, load factors and reliability indices calculated by the ANN model and ACI 440.1R are recorded as shown in Table 3. These values are utilized to draw the β–λ curves. Using the target reliability indices β_T=3.0, β_T=3.5, and β_T=4.0, the horizontal lines $\beta=\beta_T$ are determined. Then, the target load factors λ_T are calculated from the intersections between β–λ curves and $\beta=\beta_T$ as can be seen from Figure 11. In the case of ANN, the target load factors λ_T of specimen COMP-00 corresponding to the target reliability indices of 3.0, 3.5, and 4.0 are 1.265, 1.423, and 1.59 as shown in Figure 11-a. The resistance reduction factors corresponding to these load factors are 0.79, 0.7, and 0.63, respectively. In the case of ACI (Figure 11-b), the load factor at the same target reliability index is larger than that in the case of ANN. Particularly, the load factors corresponding to the target reliability indices of 3.0, 3.5, and 4.0 are 1.33, 1.515, and 1.71. The resistance reduction factors calculated from these load factors are 0.75, 0.66, and 0.58.

Table 3. Load-scaling process of beam COMP–00

Scale factor	M_L (kNm)	M_{u_ACI} (kNm)	M_{u_ANN} (kNm)	λ_{ACI}	β_{ACI}	λ_{ANN}	β_{ANN}
1.64	40.52	45.02	40.68	1.11	2.21	1.00	1.97
1.45	36.02	45.02	40.68	1.25	2.78	1.13	2.53
1.27	31.52	45.02	40.68	1.43	3.39	1.29	3.12
1.00	24.76	45.02	40.68	1.82	4.21	1.64	4.03

Notes: M_L is applied moment; M_{u_ACI} is ultimate moment obtained from ACI; M_{u_ANN} is ultimate moment obtained from ANN; $\lambda_{ACI}= M_{u\_ACI}/M_L$; $\lambda_{ANN}= M_{u\_ANN}/M_L$; β_{ACI} are reliability indices obtained from ACI; β_{ANN} are reliability indices obtained from ANN.

Similar analyses are conducted for other beams including 2T10B, NB#12, ISO2, and N2#13G2. Results including target load factors (λ_T), and design resistance reduction factors (ϕ_d) at different β_T are presented in Figure 11, Tables 4 and 5. These tables demonstrate that the resistance reduction factors decrease significantly when the target reliability index increases. This phenomenon is attributed to the fact that to achieve higher reliability indices, the applied load-to-ultimate load should be reduced, leading to the decrease of ϕ_d. Particularly, in the case of ANN (Table 4), ϕ_d of specimens 2T10B, NB#12, ISO2, and N2#13G2 decline from 0.88 to 0.7, 0.86 to 0.68, 0.82 to 0.66, and 0.85 to 0.69, respectively, when β_T increases from 3.0 to 4.0. The average values of ϕ_d for the design of FRP RC beams can be taken as 0.84, 0.75, and 0.69 corresponding to β_T=*3.0*, β_T=*3.5*, and β_T=*4.0*. In the case of ACI (see Table 4), ϕ_d of specimens 2T10B, NB#12, ISO2, and N2#13G2 decrease from 0.76 to 0.61, 0.75 to 0.59, 0.75 to 0.6, and 0.76 to 0.61, respectively, when β_T rises from 3.0 to 4.0. In this case, the average values of ϕ_d for the design of FRP RC beams when β_T=*3.0*, β_T=*3.5*, and β_T=*4.0* are 0.75, 0.67, and 0.6, respectively. Therefore, it is obvious that the design by ACI 440.1R is more conservative than the design by ANN because there are assumptions in the calculations and inclusion of safety factors in the design

equations of ACI. In addition, the larger *CoV* in the case of ACI also reduces the reliability indices compared to those obtained from ANN. Consequently, the resistance reduction factors in the case of ACI 440.1R are smaller than those of ANN at the same target reliability index (see Table 5).

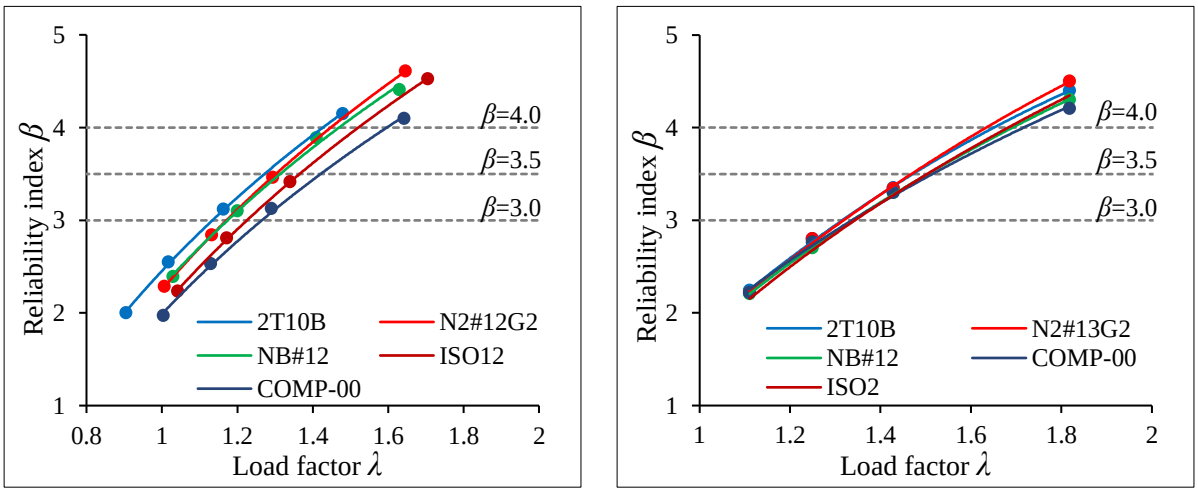

(a) Predicted by ANN (b) Predicted by ACI

Figure 11. β-λ relationships of the investigated beams

Table 4. Resistance factor for the design (ϕ_d) of FRP RC beams predicted by ANN

Beam	β_T=3.0		β_T=3.5		β_T=4.0	
	λ_T	ϕ_d	λ_T	ϕ_d	λ_T	ϕ_d
2T10B	1.132	0.88	1.27	0.79	1.425	0.70
NB#12	1.16	0.86	1.305	0.77	1.465	0.68
COMP-00	1.265	0.79	1.423	0.70	1.416	0.71
ISO2	1.225	0.82	1.37	0.73	1.52	0.66
N2#13G2	1.17	0.85	1.3	0.77	1.44	0.69
Average		0.84		0.75		0.69

Table 5. Resistance factor for the design (ϕ_d) of FRP RC beams predicted by ACI

Beam	β_T=3.0		β_T=3.5		β_T=4.0	
	λ_T	ϕ_d	λ_T	ϕ_d	λ_T	ϕ_d
2T10B	1.315	0.76	1.47	0.68	1.65	0.61
NB#12	1.34	0.75	1.505	0.66	1.69	0.59
COMP-00	1.334	0.75	1.515	0.66	1.71	0.58
ISO2	1.34	0.75	1.5	0.67	1.68	0.60
N2#13G2	1.317	0.76	1.465	0.68	1.63	0.61
Average		0.75		0.67		0.60

6.1. The Effect of Section Width b_c

The influence of b_c on the reliability indices β, the target load factor λ_T and the design resistance reduction factor ϕ_d of the investigated beam is analysed by fluctuating the values of b_c in the range from 100 mm to 500 mm. The results of the analysis are presented in Figures 12 and 13. Figures 12 demonstrate that b_c has minor effect on the relationship between reliability index and load factor. Particularly, in the case of ANN (Figures 12-a), the values of λ_T fluctuate slightly around 8.4 % (from 1.43 to 1.55), 7 % (from 1.29 to 1.38), and 5.17 % (from 1.16 to 1.22) corresponding to β_T=4.0, β_T=3.5, and β_T=3.0 when b_c changes. In the case of ACI (Figures 12-b), the effect of b_c is even smaller as shown in Figures 12-b. The values of load factors vary negligibly around 4.29 % (from 1.63 to 1.7), 3.45 % (from 1.45 to 1.5), and 3.1 % (from 1.29 to 1.33) corresponding to β_T=4.0, β_T=3.5, and β_T=3.0 when b_c changes. Figure 13 illustrates that b_c has negligible influences on the resistance reduction factors (ϕ_d). In the case of ANN (Figure 13-a), the maximum variation of ϕ_d is around 8 % when b_c varies from 100 mm to 500 mm, In particular, they fluctuate in the range from 0.65 to 0.698, 0.724 to 0.770, and 0.82 to 0.86 corresponding to β_T=4.0, β_T=3.5, and β_T=3.0. Figure 13-b demonstrates the effects of b_c on the values of ϕ_d predicted by ACI 440.1R.

As can be seen from this figure, ϕ_d fluctuates from 0.588 to 0.613, which is about 4.2 % when β_T=4.0. When β_T=3.5, ϕ_d changes slightly by 3.5 % from 0.662 to 0.686. When β_T=3.0, ϕ_d varies from 0.751 to 0.775, which is approximately 3.1 %. These values illustrate that the influence of b_c on ϕ_d is not significant. Figure 13-c demonstrates that the resistance reduction factors obtained by ANN (ϕ_{d_ANN}) are always larger than those obtained from ACI (ϕ_{d_ACI}). When β_T increases from 3.0 to 4.0, the values of $\phi_{d\_ANN}/\phi_{d\_ACI}$ fluctuate in the range from 1.07 to 1.15. In average, the values of ϕ_d obtained from ANN is approximately 1.1 times higher than those of ACI. This phenomenon can be attributed to the larger value of *CoV* in the case of ACI compared to that of ANN. When *CoV* is large, the ultimate moment of the investigated beams vary in a wider range, leading to higher failure probability and smaller design resistance reduction factor ϕ_d.

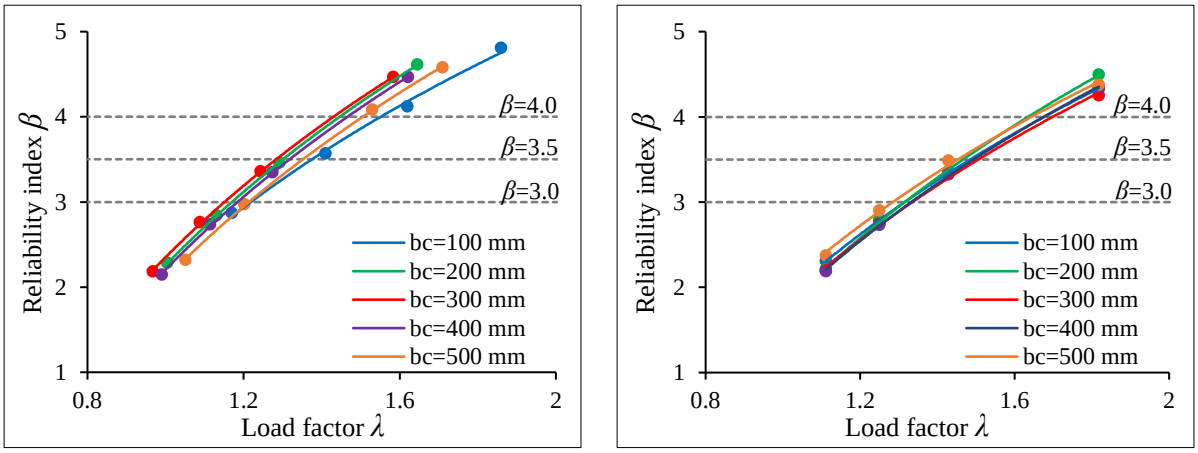

(a) Predicted by ANN (b) Predicted by ACI

Figure 12. The effect of b_c on β-λ relationship of the investigated beam

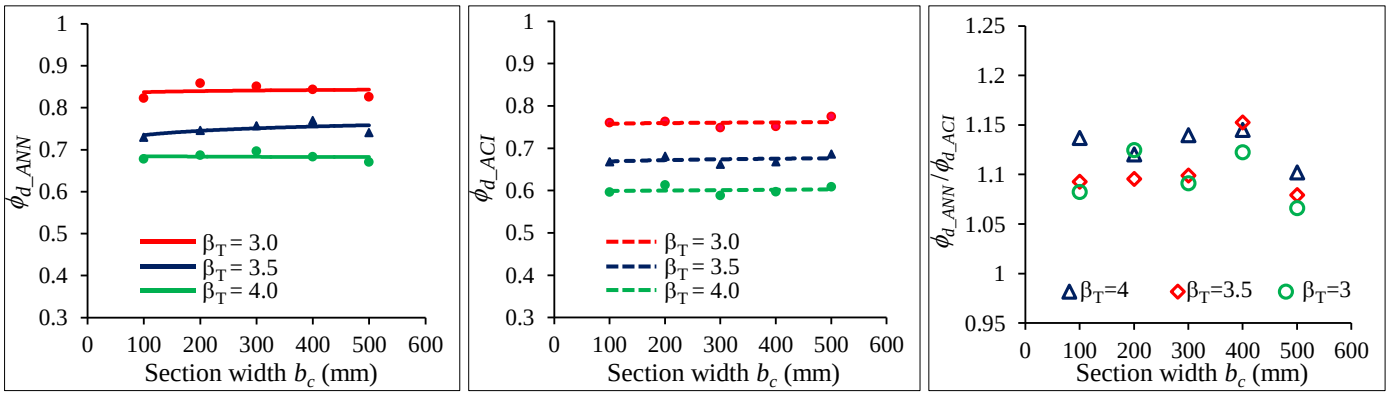

a) ϕ_{d_ANN} b) ϕ_{d_ACI} c) $\phi_{d\_ANN}/\phi_{d\_ACI}$

Figure 13. The effect of b_c on the reduction resistance factor for the design of the investigated beam

6.2. The Effect of Section Height h_c

Figures 14 and 15 demonstrate the effects of h_c on reliability indices β, the target load factor λ_T and the design resistance reduction factor ϕ_d of the investigated beam. As can be seen from Figure 14, h_c fluctuates in the range from 150 mm to 550 mm, and it has slight effects on the β-λ relationship. In the case of ANN (Figure 14-a), the values of load factors increase slightly from 1.42 to 1.51, from 1.27 to 1.35, and from 1.14 to 1.21 corresponding to β_T=4.0, β_T=3.5, and β_T=3.0 when h_c changes. Similarly, the effect of h_c in the case of ACI is also negligible (Figure 14-b). The values of load factors vary from 1.6 to 1.67, from 1.43 to 1.5, and from 1.29 to 1.33 corresponding to β_T=4.0, β_T=3.5, and β_T=3.0 when h_c fluctuates. The effects of h_c on the resistance reduction factors for the design of FRP RC beams is shown in Figure 15. It is obvious that the values of ϕ_d are not significantly affected by h_c when it increases from 150 mm to 550 mm. Particularly, in the case of ANN (see Figure 15-a), the values of ϕ_d fluctuate in the range from 0.667 to 0.704 when β_T=4.0, which is almost 5.6 %.

When β_T=3.5, the values of ϕ_d vary from 0.741 to 0.787, which is only about 6.2 %. Similarly, ϕ_d changes slightly about 6.1 % from 0.826 to 0.877 when β_T=3.0. Figure 15-b demonstrates the influences of h_c on the values of ϕ_d obtained from ACI 440.1R. According to this figure, ϕ_d varies by 3.1 % from 0.596 to 0.615 when β_T=4.0. When β_T decreases to

3.5, the values of ϕ_d fluctuate from 0.657 to 0.694, which is about 5.7 %. When β_T=3.0, ϕ_d changes slightly from 0.748 to 0.771, which is approximately 3.1 %. As a result, the fluctuations of ϕ_d when h_c increases from 150 mm to 550 mm are not significant. The reason of this phenomenon is that the values of h_c does not affect the distributions of samples generated in the sampling process. Therefore, h_c has little effects on the failure probability, reliability indices, and design resistance reduction factors ϕ_d. In Figure 15-c, the ratio between ϕ_d of ANN and ϕ_d of ACI when β_T=4.0, β_T=3.5, and β_T=3.0 is depicted. It can be seen from this figure that ϕ_d obtained from ANN is always larger than ϕ_d obtained from ACI. Particularly, the average value of $\phi_{d\_ANN}/\phi_{d\_ACI}$ is approximately 1.12.

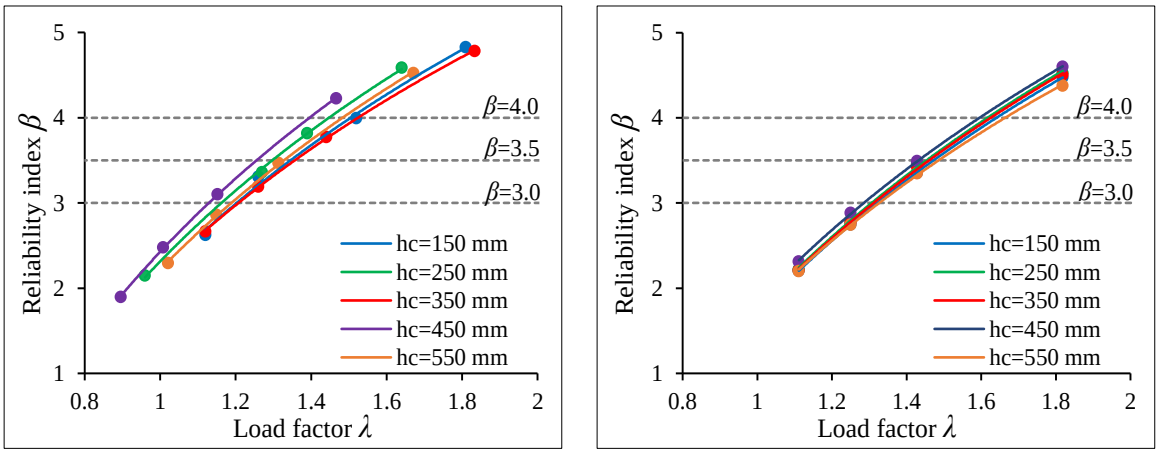

(a) Predicted by ANN (a) Predicted by ACI

Figure 14. The effect of h_c on β-λ relationship of the investigated beam

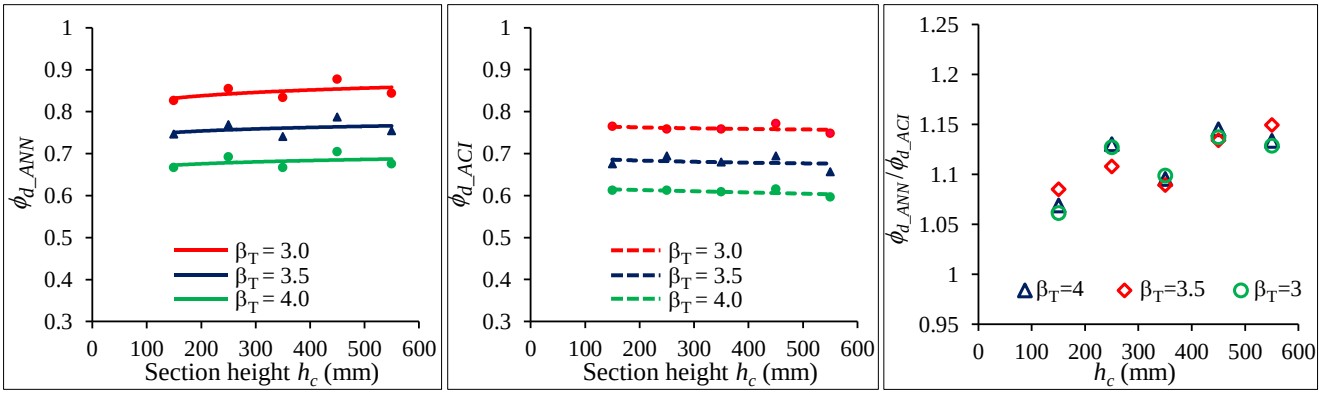

a) ϕ_{d_ANN} b) ϕ_{d_ACI} c) $\phi_{d\_ANN}/\phi_{d\_ACI}$

Figure 15. The effect of h_c on the reduction resistance factor for the design of the investigated beam

6.3. The Effect of Concrete Compressive Strength f_c

To investigate the influence of f_c on β-λ curves and the resistance reduction factor ϕ_d, the value of f_c is fluctuated in the range from 20 MPa to 100 MPa. The results of the analysis are depicted in Figures 16 and 17. In the case of ANN, β-λ curves change slightly when f_c increases from 20 MPa to 100 MPa as shown in Figure 16-a. Particularly, λ_T varies from 1.43 to 1.52 (around 7.6 %), from 1.28 to 1.39 (around 8.59 %), and from 1.16 to 1.24 (around 7.83 %) corresponding to β_T=4.0, β_T=3.5, and β_T=3.0. In the case of ACI, the effect of f_c on β-λ curves is also negligible as can be seen from Figure 16-b. According to this figure, the values of β vary slightly from 1.65 to 1.71 (around 3.64 %), from 1.46 to 1.51 (around 3.42 %), and from 1.29 to 1.34 (around 3.88 %) corresponding to β_T=4.0, β_T=3.5, and β_T=3.0, respectively. Figure 17 depicts the variation of the resistance reduction factor ϕ_d for the design of FRP RC beams when f_c changes from 20 MPa to 100 MPa.

In the case of ANN (Figure 17-a), the values of ϕ_d change from 0.66 to 0.704, 0.729 to 0.785, and 0.813 to 0.855 when β_T=4.0, β_T=3.5, and β_T=3.0, respectively. In the case of ACI 440.1R (see Figure 17-b), the values of ϕ_d also vary slightly when f_c changes from 20 MPa to 100 MPa. When β_T=4.0, ϕ_d lies in the range from 0.585 to 0.606. When β_T=3.5, ϕ_d fluctuate from 0.66 to 0.685. When β_T=3.0, ϕ_d varies from 0.746 to 0.0.775. Therefore, f_c does not affect the values of ϕ_d much. The main reason is the changes in the values of f_c does not lead to the changes in their probabilistic models.

As a result, the reliability indices and resistance reduction factors almost remain constant. In Figure 17-c, the comparison between ϕ_d obtained from ANN (denoted as ϕ_{d_ANN}) and that of ACI (denoted as ϕ_{d_ACI}) is depicted. When β_T varies from 3.0 to 4.0, $\phi_{d\_ANN}/\phi_{d\_ACI}$ ratio fluctuates in the range from 1.07 to 1.14. The average value of $\phi_{d\_ANN}/\phi_{d\_ACI}$ is approximately larger than 1.08.

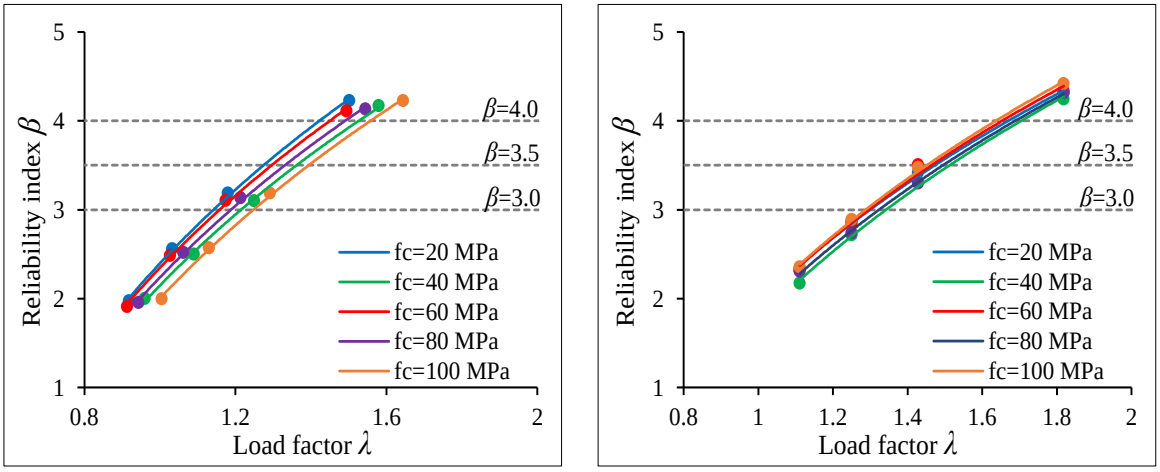

(a) Predicted by ANN (b) Predicted by ACI

Figure 16. The effect of f_c on β-λ relationship of the investigated beam

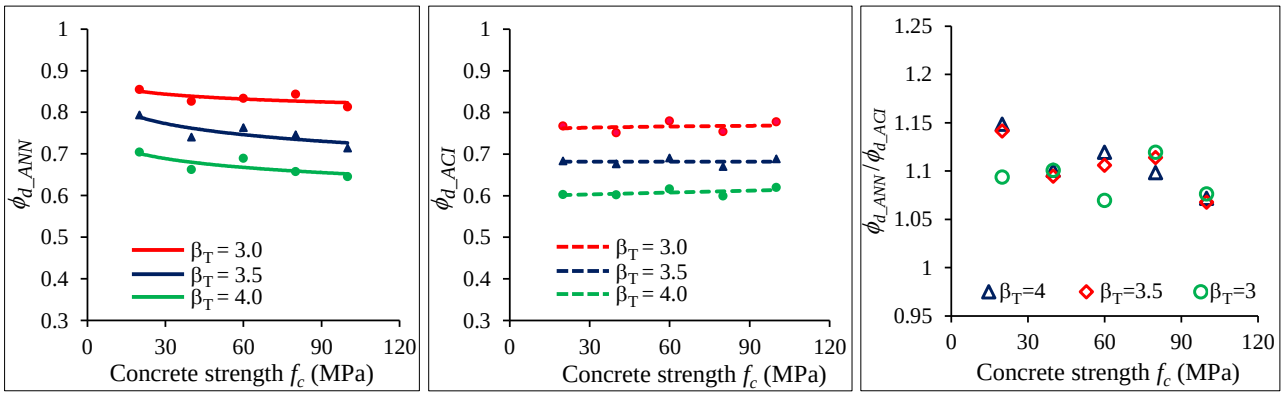

a) ϕ_{d_ANN} b) ϕ_{d_ACI} c) $\phi_{d\_ANN}/\phi_{d\_ACI}$

Figure 17. The effect of f_c on the reduction resistance factor for the design of the investigated beam.

6.4. The Effect of FRP Tensile Strength f_{fu}

The effect of FRP tensile strength f_{fu} on the reliability indices β, the target load factors λ_T and the design resistance reduction factor ϕ_d is explored in this section. To do that, the value of f_{fu} is fluctuated in the range from 500 MPa to 1250 MPa, then the analysis corresponding to each value of f_{fu} is conducted to determine the β-λ curves and the resistance reduction factors ϕ_d. The results are depicted in Figures 18 and 19. In the case of ANN (Figure 18-a), f_{fu} has negligible influence on the β-λ curves. When f_{fu} fluctuates in the range from 500 MPa to 1250 MPa, the values of λ_T vary by 6.5 % (from 1.39 to 1.48), 4 % (from 1.25 to 1.3), and 3.6 % (from 1.12 to 1.16) corresponding to β_T=4.0, β_T=3.5, and β_T=3.0. A similar trend has been observed in the case of ACI 440.1R (Figure 18-b) as the values of λ_T fluctuate slightly from 1.55 to 1.69, from 1.38 to 1.47, and from 1.22 to 1.32 when β_T=4.0, β_T=3.5, and β_T=3.0, respectively.

The values of resistance reduction factors are also affected slightly by f_{fu} as shown in Figure 19. According to this figure, when f_{fu} changes from 500 MPa to 1250 MPa, the average values of ϕ_d corresponding to β_T=4.0, β_T=3.5, and β_T=3.0 are 0.7, 0.77, 0.87 in the case of ANN (Figure 19-a). In addition, when f_{fu} varies, the values of ϕ_d fluctuates from 0.675 to 0.719, 0.769 to 0.8, 0.862 to 0.89 corresponding to β_T=4.0, β_T=3.5, and β_T=3.0. In the case of ACI 440.1R (Figure 19-b), these values are 0.62, 0.69, 0.78, corresponding to β_T=4.0, β_T=3.5, and β_T=3.0 when f_{fu} varies. Particularly, when β_T=4.0, β_T=3.5, and β_T=3.0, ϕ_d changes from 0.592 to 0.645, 0.68 to 0.724, and 0.757 to 0.819, respectively. These numbers demonstrate that the resistance reduction factors obtained from ANN are relatively larger than those obtained from ACI 440.1R. More details can be found in Figure 19-c. It can be seen from this figure that $\phi_{d\_ANN}/\phi_{d\_ACI}$ is approximately larger than 1.06.

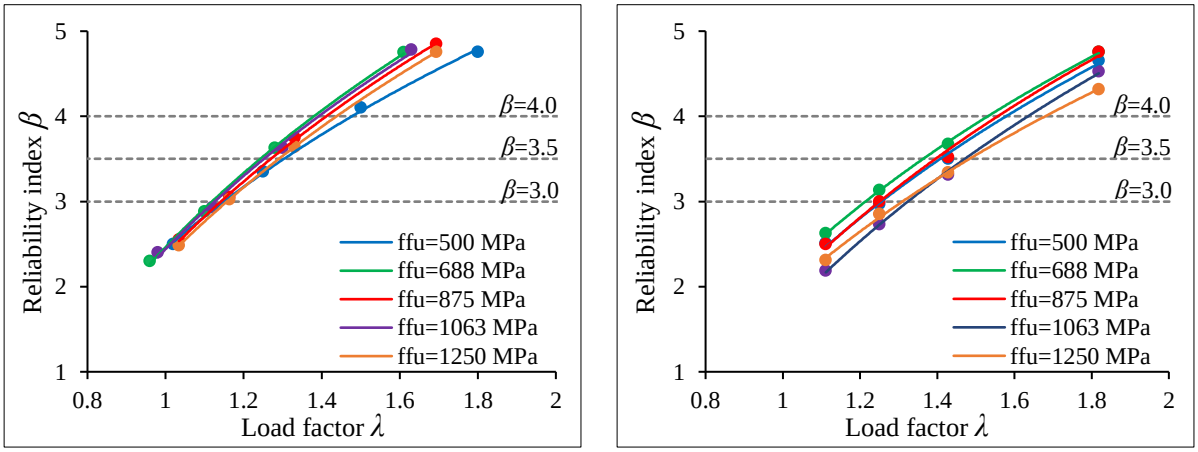

(a) Predicted by ANN (b) Predicted by ACI

Figure 18. The effect of f_{fu} on β-λ relationship of the investigated beam

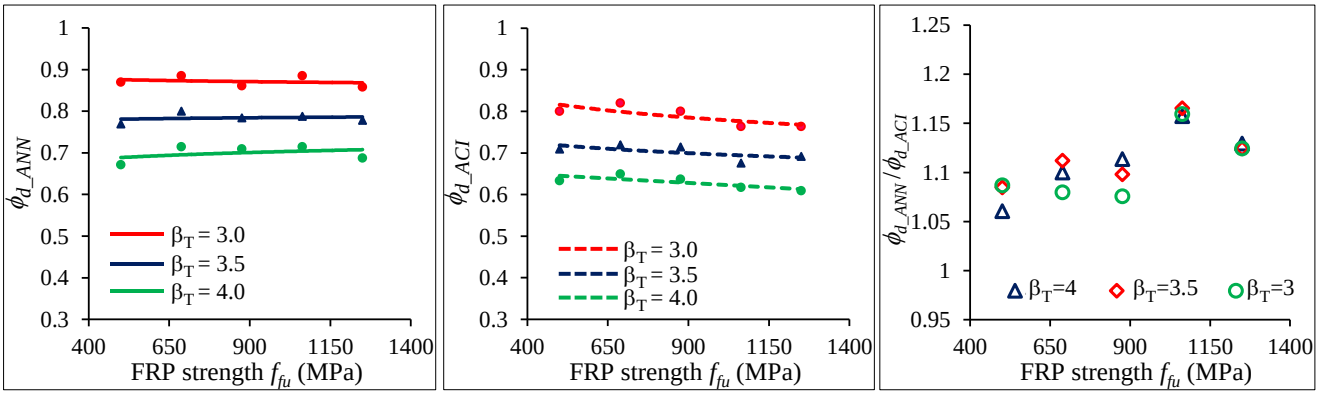

a) ϕ_{d_ANN} b) ϕ_{d_ACI} c) $\phi_{d\_ANN}/\phi_{d\_ACI}$

Figure 19. The effect of f_{fu} on the reduction resistance factor for the design of the investigated beam.

7. Conclusions

In this paper, an ANN model is trained in MATLAB by using the database of 200 beams collected from previous experimental studies to predict the moment capacity and the failure modes of FRP RC beams. The accuracy of the trained ANN model is verified with the experimental results and the design equations of ACI 440.1R. Besides, a MATLAB code is developed and integrated with the trained ANN model and the equations of ACI 440.1R to conduct the reliability analysis and calibrate the resistance reduction factors of FRP RC beams. Based on the results obtained from the analysis, some conclusions are drawn as follows:

- The trained ANN model can predict the moment capacity of FRP RC beams quite precisely since the mean and *CoV* of M_{test}/M_{ANN} ratio are only 0.98 and 0.12, respectively. In addition, the trained ANN model also captures well the failure modes of the FRP RC beams because it can predict correctly the concrete crushing and FRP rupture failure modes up to 100% and 92.7%, respectively, compared to the experimental results.
- The design equations of ACI 440.1R can also estimate the ultimate moment of FRP RC beams quite accurately with the mean and *CoV* of M_{test}/M_{ANN} ratio of 0.97 and 0.17, respectively. However, it is still less precise than the results from the trained ANN model because the *CoV* of M_{test}/M_{ACI} ratio obtained from ACI 440.1R is larger than that of the ANN model (0.17 compared to 0.12).
- The time of the reliability analysis in the case of ANN is almost the same as that in the case of ACI 440.1R, which demonstrates that ANN can be a potential approach to replace the finite element method or discrete element method when conducting reliability analysis to save computational cost.
- Based on the results of the reliability analysis, it has been found that the resistance reduction factors for the design of FRP RC beams in the case of ACI 440.1R can be taken as 0.6, 0.65, and 0.75 corresponding to β_T = 4.0, β_T = 3.5, and β_T = 3.0. In the case of ANN, these values can be taken as 0.65, 0.75, and 0.8 when β_T =4.0, β_T = 3.5, and β_T = 3.0, respectively.

8. Declarations

8.1. Author Contributions

Conceptualization, H.T. and T.N.T.; methodology, H.T. and T.N.T.; software, H.T.; validation, H.T., T.N.T., and Q.T.B.N.; formal analysis, H.T.; investigation, H.T.; resources, H.T., T.N.T., and Q.T.B.N.; data curation, H.T., T.N.T., and Q.T.B.N.; writing—original draft preparation, H.T.; writing—review and editing, H.T., T.N.T., and Q.T.B.N.; visualization, H.T., T.N.T., and Q.T.B.N.; supervision, H.T. and T.N.T.; project administration, H.T. and T.N.T.; funding acquisition, H.T. All authors have read and agreed to the published version of the manuscript.

8.2. Data Availability Statement

The data presented in this study are available in the article.

8.3. Funding and Acknowledgments

The financial supports from Van Lang University and Cong Ty TNHH Xay Dung Cong Nghe Hop Kim (ALTECK Ltd.) is gratefully acknowledged.

8.4. Conflicts of Interest

The authors declare no conflict of interest.

9. References

[1] Ganesan, N., Abraham, R., Raj, S. D., & Namitha, K. (2016). Effect of fibres on the strength and behaviour of GPC columns. Magazine of Concrete Research, 68(2), 99–106. doi:10.1680/jmacr.15.00049.

[2] Maranan, G. B., Manalo, A. C., Benmokrane, B., Karunasena, W., & Mendis, P. (2016). Behavior of concentrically loaded geopolymer-concrete circular columns reinforced longitudinally and transversely with GFRP bars. Engineering Structures, 117, 422–436. doi:10.1016/j.engstruct.2016.03.036.

[3] Nagan, S., & Karthiyaini, S. (2014). A study on load carrying capacity of fly ash based polymer concrete columns strengthened using double layer GFRP wrapping. Advances in Materials Science and Engineering, 312139. doi:10.1155/2014/312139.

[4] Al-Gburi, M., Alhayani, A. A., & Almssad, A. (2025). Artificial Neural Network Model for Evaluating Load Capacity of RC Deep Beams. Buildings, 15(8), 1371. doi:10.3390/buildings15081371.

[5] Tran, H., & Nguyen-Thoi, T. (2025). Flexural Behavior of Beams Reinforced with FRP Bars: Test Database, Design Guideline Assessment, and Reliability Evaluation. Buildings, 15(18), 3373. doi:10.3390/buildings15183373.

[6] Tran, H., Nguyen-Thoi, T., & Dinh, H. B. (2025). State-of-the-Art Review of Studies on the Flexural Behavior and Design of FRP-Reinforced Concrete Beams. Materials, 18(14), 3295. doi:10.3390/ma18143295.

[7] Anas, S. M., Alam, M., & Umair, M. (2021). Experimental and numerical investigations on performance of reinforced concrete slabs under explosive-induced air-blast loading: A state-of-the-art review. Structures, 31, 428-461. doi:10.1016/j.istruc.2021.01.102.

[8] Ding, L., Dai, X., Gan, Y., & Zeng, Y. (2025). Impact of Reinforcement Corrosion on Progressive Collapse Behavior of Multi-Story RC Frames. Buildings, 15(14), 2534. doi:10.3390/buildings15142534.

[9] Li, F., Li, Y., Luo, W., Lei, C., Pan, W., & Ji, S. (2025). A new seismic strategy for strong column-weak beam design philosophy in RC frame structures. Structures, 77. doi:10.1016/j.istruc.2025.109129.

[10] Manalo, A. C., Mendis, P., Bai, Y., Jachmann, B., & Sorbello, C. D. (2021). Fiber-Reinforced Polymer Bars for Concrete Structures: State-of-the-Practice in Australia. Journal of Composites for Construction, 25(1), 05020007. doi:10.1061/(asce)cc.1943-5614.0001105.

[11] Al Hawarneh, A., Al Martini, S., Sabouni, R., Al Mzayyen, N., & Alam, M. S. (2025). Shear behavior of concrete beams reinforced with basalt FRP rebars and incorporating recycled aggregates. Structures, 78. doi:10.1016/j.istruc.2025.109250.

[12] Ali, A., Sharaky, I. A., Khalil, A. H. H., & Attia, M. M. (2025). Effect of NSM end conditions and materials on flexural response of the RC beams strengthened with novel hybrid steel-FRP bars. Case Studies in Construction Materials, 22, e04862. doi:10.1016/j.cscm.2025.e04862.

[13] Ebrahimzadeh, M., Jeddian, S., Shakiba, M., Hosseini, S. M., Bazli, M., kashani, H. K., & Rahmati, M. (2025). Effect of column height on the seismic behavior of slender FRP and steel reinforced concrete columns actively confined by AFRP strips. Structures, 80. doi:10.1016/j.istruc.2025.109719.

[14] Kadhim, A. J., & Zinkaah, O. H. (2025). Numerical and theoretical investigation for the flexural behaviour of geopolymer concrete beams reinforced with hybrid FRP /steel bars. Journal of Building Engineering, 101. doi:10.1016/j.jobe.2025.111883.

[15] Nguyen, P. D., & Dang, V. H. (2025). Shear strength of FRP - reinforced concrete deep beams: Extension of beam and arch action model based on data-driven analysis. Structures, 74. doi:10.1016/j.istruc.2025.108553.

[16] Qu, H., Hu, T., Qu, J., & Taffese, W. Z. (2025). A machine learning model based on GAN-ANN data augmentation for predicting the bond strength of FRP-reinforced concrete under high-temperature conditions. Composite Structures, 369. doi:10.1016/j.compstruct.2025.119321.

[17] Concha, N. C. (2022). Neural network model for bond strength of FRP bars in concrete. Structures, 41, 306–317. doi:10.1016/j.istruc.2022.04.088.

[18] Guo, B., Lin, X., Wu, Y., & Zhang, L. (2023). Machine learning-driven evaluation and optimisation of compression yielded FRP-reinforced concrete beam with T section. Engineering Structures, 275. doi:10.1016/j.engstruct.2022.115240.

[19] Huang, L., Chen, J., & Tan, X. (2022). BP-ANN based bond strength prediction for FRP reinforced concrete at high temperature. Engineering Structures, 257. doi:10.1016/j.engstruct.2022.114026.

[20] Murad, Y., Tarawneh, A., Arar, F., Al-Zu'bi, A., Al-Ghwairi, A., Al-Jaafreh, A., & Tarawneh, M. (2021). Flexural strength prediction for concrete beams reinforced with FRP bars using gene expression programming. Structures, 33, 3163–3172. doi:10.1016/j.istruc.2021.06.045.

[21] Attarchian, N., Aghamohammadi, R., & Nasrollahzadeh, K. (2025). Reliability-Based Calibration of Strength-Reduction Factors for Flexural Design of FRP-RC Beams Under Various Load Combinations. Journal of Composites Science, 9(4), 154. doi:10.3390/jcs9040154.

[22] Feng, L., Li, P. Da, Huang, X. X., & Wu, Y. F. (2022). Reliability-Based Design Analysis for FRP Reinforced Compression Yield Beams. Polymers, 14(22), 4846. doi:10.3390/polym14224846.

[23] Ribeiro, S. E. C., & Diniz, S. M. C. (2013). Reliability-based design recommendations for FRP-reinforced concrete beams. Engineering Structures, 52, 273–283. doi:10.1016/j.engstruct.2013.02.026.

[24] Ge, W., Zhang, F., Wang, Y., Ashour, A., Luo, L., Qiu, L., Fu, S., & Cao, D. (2024). Machine learning predictions for bending capacity of ECC-concrete composite beams hybrid reinforced with steel and FRP bars. Case Studies in Construction Materials, 21, e03670. doi:10.1016/j.cscm.2024.e03670.

[25] Shahriari, S., & Naderpour, H. (2020). Reliability assessment of shear-deficient reinforced concrete beams externally bonded by FRP sheets having different configurations. Structures, 25, 730–742. doi:10.1016/j.istruc.2020.03.048.

[26] Zhang, T., Gao, D., & Xue, C. (2024). Flexural strength prediction of concrete beams reinforced with hybrid FRP and steel bars based on machine learning. Structures, 65. doi:10.1016/j.istruc.2024.106652.

[27] He, Z., & Qiu, F. (2011). Probabilistic assessment on flexural capacity of GFRP-reinforced concrete beams designed by guideline ACI 440.1R-06. Construction and Building Materials, 25(4), 1663–1670. doi:10.1016/j.conbuildmat.2010.10.005.

[28] Zhou, Y., Zhang, J., Li, W., Hu, B., & Huang, X. (2020). Reliability-based design analysis of FRP shear strengthened reinforced concrete beams considering different FRP configurations. Composite Structures, 237. doi:10.1016/j.compstruct.2020.111957.

[29] Rahman, S. K., & Al-Ameri, R. (2023). Structural assessment of Basalt FRP reinforced self-compacting geopolymer concrete using artificial neural network (ANN) modelling. Construction and Building Materials, 397. doi:10.1016/j.conbuildmat.2023.132464.

[30] Tran, V. L., Thai, D. K., & Kim, S. E. (2019). Application of ANN in predicting ACC of SCFST column. Composite Structures, 228. doi:10.1016/j.compstruct.2019.111332.

[31] Yu, Y., Fang, G.-H., Kurda, R., Sabuj, A. R., & Zhao, X.-Y. (2024). An agile, intelligent and scalable framework for mix design optimization of green concrete incorporating recycled aggregates from precast rejects. Case Studies in Construction Materials, 20, e03156. doi:10.1016/j.cscm.2024.e03156.

[32] ACI440.1R-15. (2015). Guide for the Design and Construction of Structural Concrete Reinforced with Fiber - Reinforced Polymer (FRP) Bars. American Concrete Institute, Michigan, United States.

[33] Abed, F., Al-Mimar, M., & Tello, N. (2019). Evaluation of BFRP RC beams under flexure. 2019 Advances in Science and Engineering Technology International Conferences (ASET), 1–4. doi:10.1109/icaset.2019.8714344.

[34] Benmokrane, B., Chaallal, O., & Masmoudi, R. (1996). Flexural response of concrete beams reinforced with FRP reinforcing bars. ACI Structural Journal, 93(1), 46–55. doi:10.14359/9839.

[35] Barris, C., Torres, L., Comas, J., & Miàs, C. (2013). Cracking and deflections in GFRP RC beams: An experimental study. Composites Part B: Engineering, 55, 580–590. doi:10.1016/j.compositesb.2013.07.019.

[36] El-Nemr, A., Ahmed, E. A., & Benmokrane, B. (2013). Flexural Behavior and Serviceability of Normal-and High-Strength Concrete Beams Reinforced with Glass Fiber-Reinforced Polymer Bars. ACI Structural Journal, 110(6), 110-S88.

[37] Mostafa, O. M., Rahman, M. K., Al-Zahrani, M. M., Adekunle, S. K., Al-Osta, M. A., & Najamuddin, S. K. (2023). Flexural behavior and bond coefficient of BFRP bar reinforced normal and high strength concrete beams. Construction and Building Materials, 401. doi:10.1016/j.conbuildmat.2023.132896.

[38] Shamass, R., & Cashell, K. A. (2020). Experimental investigation into the flexural behaviour of basalt FRP reinforced concrete members. Engineering Structures, 220. doi:10.1016/j.engstruct.2020.110950.

[39] Almusallam, T. H., Al-Salloum, Y. A., Alsayed, S. H., & Amjad, M. A. (1997). Behavior of concrete beams doubly reinforced by FRP bars. Proceedings of the third international symposium on non-metallic (FRP) reinforcement for concrete structures (FRPRCS-3), Sapporo, Japan, 14–16 October 1997, Volume 2, 471–478.

[40] Wang, Z., Xie, J., Li, J., Liu, P., Shi, C., & Lu, Z. (2022). Flexural behaviour of seawater–sea sand concrete beams reinforced with GFRP bars: Effects of the reinforcement ratio, stirrup ratio, shear span ratio and prestress level. Journal of Building Engineering, 54. doi:10.1016/j.jobe.2022.104566.

[41] Muhammad, M. A., & Ahmed, F. R. (2023). Evaluation of deflection and flexural performance of reinforced concrete beams with glass fiber reinforced polymer bars. Case Studies in Construction Materials, 18, e01855. doi:10.1016/j.cscm.2023.e01855.